Monthly Notices of the ROYAL ASTRONOMICAL SOCIETY

MNRAS **459,** 1082–1096 (2016) doi:10.1093/mnras/stw720
Advance Access publication 2016 March 28

Models of cuspy triaxial stellar systems – IV. Rotating systems

D. D. Carpintero[1,2]★ and J. C. Muzzio[1,2]

[1]*Facultad de Ciencias Astronómicas y Geofísicas, Universidad Nacional de La Plata, Paseo del Bosque S/N, 1900 La Plata, Argentina*
[2]*Instituto de Astrofísica de La Plata CONICET-UNLP, Paseo del Bosque S/N, 1900 La Plata, Argentina*

Accepted 2016 March 23. Received 2016 March 7; in original form 2015 December 23

ABSTRACT

We built two self-consistent models of triaxial, cuspy, rotating stellar systems adding rotation to non-rotating models presented in previous papers of this series. The final angular velocity of the material is not constant and varies with the distance to the centre and with the height over the equator of the systems, but the figure rotation is very uniform in both cases. Even though the addition of rotation to the models modifies their original semi-axes ratios, the final rotating models are considerably flattened and triaxial. An analysis of the orbital content of the models shows that about two-thirds of their orbits are chaotic yet the models are very stable over intervals of the order of one Hubble time. The bulk of regular orbits are short-axis tubes, while long-axis tubes are replaced by tubes whose axes lie on the short-long axes plane, but do not coincide with the major axis. Other types of regular orbits that do not appear in non-rotating systems, like horseshoes and orbits that cross themselves, are also found in the present models. Finally, our frequency maps show empty regions where studies of orbits on fixed potentials found orbits, a likely consequence of the self-consistency of our models that excludes them.

Key words: methods: numerical – galaxies: elliptical and lenticular, cD – galaxies: kinematics and dynamics.

1 INTRODUCTION

It is relatively easy to obtain self-consistent models of spherical or disc-like stellar systems with simple numerical (e.g. King models) or even analytical tools (e.g. Schuster or Plummer models), as explained in textbooks like the one by Binney & Tremaine (2008). Models of elliptical galaxies are much more difficult to build, however, as there is observational evidence, both statistical (see e.g. Ryden 1996) and on individual galaxies (see e.g. Statler et al. 2004), that shows that at least some ellipticals are triaxial, and full-fledged 3D models demand resorting to special techniques. Besides, surface brightness studies of ellipticals tend to show central cusps (see e.g. Crane et al. 1993; Moller, Stiavelli & Zeilinger 1995), that reveal the presence of mass concentrations and probably black holes, and triaxial and cuspy potentials favour the appearance of chaotic orbits (see e.g. Siopis & Kandrup 2000; Kandrup & Siopis 2003) further complicating model building for those objects.

Two main methods are employed to build self-consistent models of elliptical galaxies: the one due to Schwarzschild (1979) and the *N*-body method, originally proposed by Sparke & Sellwood (1987) to build a bar and later on applied to ellipticals by Voglis, Kalapotharakos & Stavropoulos (2002). The former chooses a potential-density pair, builds a library of orbits in that potential and determines the fraction of each type of orbit needed to obtain the corresponding density. The *N*-body method adopts an initial distribution of point masses and integrates the equations of motion until an equilibrium distribution is reached; a smooth and constant potential is then fitted to that distribution and the positions and velocities of the bodies are used to investigate the orbits in that potential.

Schwarzschild (1993) himself noted the difficulty to include chaotic orbits in models built with his method, which turned out to evolve over intervals of the order of a Hubble time, and the problem became even more serious when cuspy models were adopted (see e.g. Merritt & Fridman 1996). Although it was suggested that models containing chaotic orbits could not be stable (e.g. Siopis & Kandrup 2000), perfectly stable models with large fractions of chaotic orbits were built with the *N*-body method (Voglis et al. 2002; Kalapotharakos & Voglis 2005; Muzzio, Carpintero & Wachlin 2005; Aquilano et al. 2007), including cuspy ones (Muzzio, Navone & Zorzi 2009). In fact, Muzzio et al. (2005) argued that there was no physical constrain to build self-consistent stable models with chaotic orbits and that the problem dealt with the method of Schwarzschild (1979) itself. A comprehensive recent discussion of this matter can be found in the paper by Vasiliev & Athanassoula (2012).

The present series of papers uses the *N*-body method to build models of cuspy triaxial stellar systems and investigate their stability and orbital content, both regular and chaotic. In our first paper,

★E-mail: ddc@fcaglp.unlp.edu.ar

Zorzi & Muzzio (2012) built models resembling E2, E3, E4 and E5 galaxies and they showed that they were extremely stable over intervals of the order of a Hubble time, even though they contained fractions of chaotic orbits that exceeded 75 per cent. The regular orbits of those models were studied, in our second paper, by Muzzio, Navone & Zorzi (2013), and they found that most of those orbits were short-axis tubes (SATs), that the fraction of long-axis tubes (LATs) decreased from the E2 through the E5 models and that most of the boxes were resonant orbits, i.e. boxlets. A curious puzzle was posed by the work of Holley-Bockelmann et al. (2001) who, using the *N*-body method, built cuspy triaxial models with essentially no chaotic orbits, so that we reexamined their investigation in the third paper of our series (Carpintero, Muzzio & Navone 2014). We found that their discrepancy with the other *N*-body works had two causes: their use of a poor method to detect chaos and a velocity distribution in their model much more isotropic than that of other authors (low angular momentum orbits are more likely to be chaotic).

Now, all our previous models are either non-rotating or have exceedingly slow figure rotation, but rotation is a key ingredient of the dynamics of elliptical galaxies, and the pioneer works of Bertola & Capaccioli (1975) and Illingworth (1977) showed that they have angular momentum, even though the resulting rotation is small enough that in most cases the ellipticity of those galaxies cannot be attributed to the rotation itself.

All the investigations performed using the *N*-body method found large fractions of chaotic orbits in the non-rotating or very slowly rotating systems, and the comparison done by Muzzio (2006) of his rotating model with the same non-rotating one of Muzzio et al. (2005) suggests that rotation should increase those fractions. The works of Schwarzschild (1982), and Deibel, Valluri & Merritt (2011) are among the few in which a rotating model is used to study the dynamics of elliptical galaxies, but the former does not mention chaotic orbits and the latter does not accept that they could contribute significantly to a stable stellar system. The difficulties of the method of Schwarzschild to accommodate chaotic orbits have been mentioned above; besides, Deibel et al. (2011) do not use a self-consistent model, but only investigate orbits in a rotating triaxial generalization of the potential of Dehnen (1993). The recent work of Vasiliev & Athanassoula (2015) is a welcome addition to the subject but, although they indicate the presence of chaoticity in their models and that in general it increased with pattern speed, the information they provide on chaos is rather scanty.

Thus, we decided to try to build self-consistent, rotating, cuspy, triaxial models using the *N*-body method, in order to find out the degree of chaos that such models harbour and the distribution of the regular orbits, and that is the subject of this paper. The following section describes the numerical techniques we used to build our models, and their stability is investigated in Section 3. Section 4 describes the matter and figure rotation of the models, and Section 5 analyzes its orbital composition, both chaotic and regular. Finally, our conclusions are presented in Section 6.

2 BUILDING ROTATING MODELS

In order to create stable, cuspy, rotating triaxial models, we take the already stable, cuspy and triaxial models dubbed E2a and E5a of the first paper of this series (Zorzi & Muzzio 2012), containing each one $N \simeq 10^6$ bodies. In these models, and in the rest of this work, the gravitational constant $G = 1$, the total mass $M = 1$ and the crossing time $T_{\rm cr}$ is equivalent to about 1/200 of the Hubble time. The slope γ of the cusp in both models, computed as the slope of the $\log \rho(r)$ versus $\log r$ line for the innermost 10 000 particles binned in bins of 100 particles each, is $\gamma \simeq -1$. The semi axes $a > b > c$ obtained from the 80 per cent most tightly bound particles are in the ratios $b/a = 0.877$, $c/a = 0.826$ for the E2a model, and $b/a = 0.814$, $c/a = 0.515$ for the E5a model. The triaxiality of the E2a model is $T \equiv (a^2 - b^2)/(a^2 - c^2) = 0.73$, whereas that of the E5a model is $T = 0.46$.

We perform the *N*-body integrations with the self-consistent field (SCF) code of Hernquist & Ostriker (1992), the same used by Zorzi & Muzzio (2012) to build their models. The code solves the Poisson's equation by expanding the density and the potential in a set of basis functions chosen in such way that the lowest order term corresponds to the model of Hernquist (1990). The motion of the bodies is followed with a time-centred leapfrog algorithm that keeps time reversibility. Zorzi & Muzzio (2012) performed several tests to choose the number of radial and angular terms in the expansion to finally adopt $n = 6$ radial and $l = 4$ angular terms for their models, and those are the same numbers we use here.

To quantify the angular momentum acquired by each model, we computed the specific angular momentum introduced by Peebles (1971):

$$\lambda = \frac{L\sqrt{|E|}}{GM^{2.5}}, \tag{1}$$

where L and E are the total angular momentum and energy of the model, respectively.

In order to add rotation while maintaining the triaxiality and the 'cuspiness' of the models, we proceeded in the following way. First, we gave to each model a certain amount of rotation by adding to each particle at position (x_i, y_i, z_i) and with velocity $(\dot{x}_i, \dot{y}_i, \dot{z}_i)$ an angular velocity $\Omega\, \boldsymbol{e}_z$, i.e.

$$\begin{aligned} \dot{x}_i' &= \dot{x}_i - \Omega\, y_i, \\ \dot{y}_i' &= \dot{y}_i + \Omega\, x_i, \\ \dot{z}_i' &= \dot{z}_i. \end{aligned} \tag{2}$$

Now, this simple recipe has a major flaw: it changes the energy of the model, which should be kept in order to maintain as much as possible its other characteristics. One way to proceed is to subtract from the velocity modulus of each particle an amount necessary to conserve the total energy after applying the rotation. The subtracted fraction $0 < k < 1$ should be the same for each particle in order to keep the kinematical structure of the model. One then has, equalizing the initial and final kinetic energies,

$$\begin{aligned} &\frac{1}{2}\sum_{i=1}^{N} m_i \left(\dot{x}_i^2 + \dot{y}_i^2\right) \\ &= \frac{1}{2}\sum_{i=1}^{N} m_i \left[k^2\left(\dot{x}_i^2 + \dot{y}_i^2\right) + 2k\Omega(x_i\dot{y}_i - y_i\dot{x}_i) + \Omega^2\left(x_i^2 + y_i^2\right)\right], \end{aligned} \tag{3}$$

where m_i is the mass of the ith particle, and N is the number of particles. Solving for k, it may happen that the resulting quadratic polynomial has imaginary roots. This means that the amount of rotational energy injected into the system is so large that it does not allow us to recover the initial kinetic energy (that is, there are particles which must have less than zero velocity to achieve that). In any other case, since the linear coefficient $\sum_i m_i \Omega(x_i\dot{y}_i - y_i\dot{x}_i)$ is approximately zero for a non-rotating system, we expect that the two roots be opposite each other. Moreover, calling a the coefficient that multiplies k^2 and c the independent term, it can be easily seen that $|c| < |a|$, so that the moduli of the roots will be less than 1.

Thus, except for the imaginary case, a unique value $0 < k < 1$ is expected among the roots, as was always the case. With the value of k, the new velocities are computed by means of

$$\begin{aligned}\dot{x}_i' &= k\dot{x}_i - \Omega\, y_i,\\ \dot{y}_i' &= k\dot{y}_i + \Omega\, x_i,\\ \dot{z}_i' &= k\dot{z}_i.\end{aligned} \tag{4}$$

As already said, with this procedure only a maximum amount of angular velocity can be applied to a given model. For example, the rotation that could be added to the E2a model amounted to $\Omega = 0.594\,95$, whereas that of the E5a model was $\Omega = 0.858\,70$. Thus, we tried to add more angular momentum in the following way.

We first let each model relax for 50 $T_{\rm cr}$, using the SCF code. After that, we aligned the coordinate axes with the semi axes of the inertia tensor of the 80 per cent most tightly bound particles of each model, so that the x-axis coincided with the semimajor axis and the z-axis with the semiminor axis, and eliminated the particles with positive energy and the 2 per cent of the remainder that have energies closer to zero.

Then, we added a new amount of angular velocity. Since to do this we cannot follow the abovementioned procedure (a fraction of the velocities of the particles are already part of the angular motion, which we do not want to subtract), we included in the computation the old angular velocity, dubbed now Ω_0, yielding

$$\begin{aligned}&\frac{1}{2}\sum_{i=1}^{N} m_i\left(\dot{x}_i^2 + \dot{y}_i^2\right)\\ &= \frac{1}{2}\sum_{i=1}^{N} m_i\left\{k^2\left(\dot{x}_i^2 + \dot{y}_i^2\right) + 2k\Omega(x_i\dot{y}_i - y_i\dot{x}_i)\right.\\ &\quad\left. - \left[\left(\Omega_0^2 - \Omega^2\right)\left(x_i^2 + y_i^2\right) + 2\Omega_0(x_i\dot{y}_i - y_i\dot{x}_i)\right]\right\}.\end{aligned} \tag{5}$$

Now the quadratic polynomial can have roots of different moduli and, in principle, with the same sign. Nevertheless, physically we expect that the reduction in energy by decreasing the velocities should be possible (so two negative roots are not expected), and that only one way to do it is feasible (so two positive roots are not expected either). Thus, the resulting roots should be one positive and one negative (which was always the case). Once the velocities have been reduced again using equation (5), the whole procedure is repeated (including the rotation of the axes and the relaxation) until the amount of angular motion to be added cannot be made much different from zero.

For the E2a model, the second introduction of angular momentum was the last to produce a significant growth of λ, whereas in the case of the E5a model, it was the third one. The final values were $\lambda = 0.124$ for the E2a model, and $\lambda = 0.178$ for the E5a model.

Then, we let the models relax during 200 $T_{\rm cr}$ (about a Hubble time); the final snapshot was again rotated using the moments of the inertia tensor of the 80 per cent most tightly bound particles. These last systems (one for each model) were evolved during an additional interval of 300 $T_{\rm cr}$ in order to verify their stability. For each of the two models, the snapshot corresponding to 100 $T_{\rm cr}$ of this last evolution was the one used to study and classify the respective orbital contents; we call them E2af and E5af, respectively, for brevity.

Fig. 1 shows the kinematic and structural characteristics of the E2af model. In this figure, the abscisae q stands for the ellipsoidal radius

$$q = \left(\frac{x^2}{a^2} + \frac{y^2}{b^2} + \frac{z^2}{c^2}\right)^{1/2}, \tag{6}$$

where a, b and c are the semi axes of the model, computed following the method of Dubinski & Carlberg (1991), as adapted by Holley-Bockelmann et al. (2001); Q, on the other hand, is the same as q but projected on to the coordinate planes. The abscisae $M(r)/M$ is the mass interior to radius r in units of the total mass of the model. The upper-left panel shows the density profile of the model, computed using ellipsoidal shells with constant axial ratios taken at the half-mass radius. As can be seen, the rotation has not substantially affected the cusp of the model ($\gamma = -1.023 \pm 0.020$, computed from the densities of the 10 000 innermost particles binned in 100 intervals of distance to the centre). The upper-right panel shows the axial ratios, computed in shells each containing 3 per cent of the particles, previously sorted by energy. The ratios of the semi axes of the shell containing 81 per cent of the mass in its interior are $b/a = 0.939$ and $c/a = 0.791$, in good agreement with the values that correspond to the 80 per cent most tightly bound bodies ($b/a = 0.925$, $c/a = 0.823$, $T = 0.447$), i.e. the parameters used in our previous works. Comparing these values with those of the original E2a model, we can see that the b/a ratio has increased, whereas the c/a ratio and the triaxiality have decreased. The bottom panels show the kinematical profiles, in which $\sigma_i^2 = \langle v_i^2\rangle - \langle v_i\rangle^2$, where i is a Cartesian direction x, y or z in the left-hand panel, and r (radial) or t (tangential) direction in the right-hand panel. The anisotropy parameter $\beta = 1 - \sigma_{\rm t}^2/(2\sigma_{\rm r}^2)$. Fig. 2 shows the same characteristics but for the E5af model. Again, the cusp is well preserved ($\gamma = -0.956 \pm 0.023$). In this case, for the same shell as before, $b/a = 0.916$, $c/a = 0.602$, while for the 80 per cent most tightly bound particles, $b/a = 0.896$, $c/a = 0.641$ and $T = 0.335$, i.e. both axial ratios have increased and the triaxiality decreased with respect to the E5a model. It might seem odd that rotation has not made the model flatter, but it should be recalled that the process that led from the non-rotating to the rotating model implied considerable changes in structure of the former. For example, about 30 per cent of the original particles were eliminated because they increased their energies beyond the established limits, and the a semi axis was reduced to about half its initial size.

In order to estimate the meaning of our length unit (l.u.) and time unit (t.u.) for real galaxies, we computed the effective radii $R_{\rm e}$ from the (x, z) projection (0.142 and 0.0794 l.u., respectively, for the E2af and E5af models) and the central radial velocity dispersion σ_0 from the y components of the velocities of the 10 000 particles closer to the centre on that projection (0.987 and 1.099 l.u./t.u., respectively, for the E2af and E5af models). As in our previous work (Aquilano et al. 2007; Muzzio et al. 2009; Zorzi & Muzzio 2012), we chose for comparison galaxies NGC1379 and NGC4697 (Forbes & Ponman 1999; Napolitano et al. 2005), whose mass-to-light ratio gradients are zero. Comparing their observed values of $R_{\rm e}$ (2.5 and 5.7 kpc, respectively) and σ_0 (128 and 180 km s^{-1}, respectively) with those from our models, we conclude that values between about 18 and 72 kpc can be used as our l.u. and values between about 0.14 and 0.44 Gyr as our t.u. Then, the Hubble time can be estimated as between 32 and 100 t.u., or between 180 and 290 $T_{\rm cr}$, and we will adopt a value of 250 $T_{\rm cr}$, hereafter.

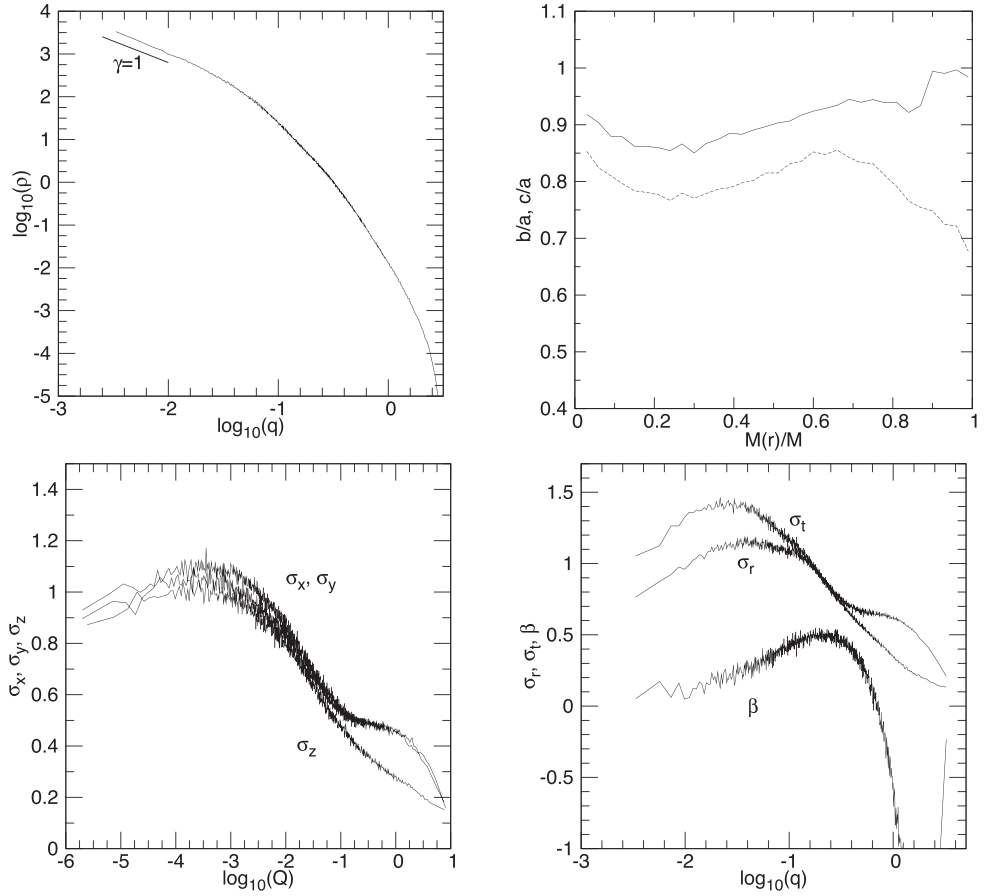

Figure 1. Structural and kinematical properties of model E2af; q is the ellipsoidal radius, Q the projected ellipsoidal radius, and $M(r)/M$ is the mass interior to r in units of the total mass. Upper left: density profile; a short segment with slope -1 was added for reference. Upper right: axial ratios; the upper curve corresponds to b/a and the lower one to c/a. Lower left: projected velocity dispersions along the main axes; upper, intermediate and lower curves correspond, respectively, to σ_x, σ_y and σ_z. Lower right: tangential and radial velocity dispersions and velocity anisotropy parameter β.

3 STABILITY OF THE MODELS

We used the final $300T_{\rm cr}$ runs to check for systematic changes in the density $\rho_{\rm c}$ of the innermost 10 000 particles, the moments of inertia X, Y and Z for each axis, and γ. To improve the precision, straight lines were fitted to the results obtained every $25T_{\rm cr}$ and we obtained the percentage variation corresponding to $250T_{\rm cr}$, i.e. one Hubble time according to our estimate. The results are presented in Table 1 and the changes are very small, indeed. Moreover, as we have shown before (Aquilano et al. 2007; Muzzio et al. 2009; Zorzi & Muzzio 2012), even those tiny variations are most likely not real but due to relaxation effects of the N-body code (Hernquist & Barnes 1990).

Nevertheless, since our models are rotating, what is conserved is not the energy of a particle in the fixed reference frame of the N-body code, but its energy in the frame that rotates with the ellipsoidal figure, i.e. the Jacobi integral (leaving aside the numerical relaxation effects, of course). Therefore, even though we eliminated the particles with positive, and slightly negative, energy in the former reference frame, there are still particles that can escape from the system. As explained by Binney & Tremaine (2008), particles that have values of the Jacobi integral larger than the value of the effective potential at the L_1 and L_2 Lagrangian points or that are initially outside the contour through those points, can *in principle* escape from the system but, due to the protective effect of the Coriolis force, that does not mean that those particles will *necessarily* escape. We obtained the limiting values of the Jacobi integral as -1.113 and -2.042, respectively, for the E2af and E5af models, and found that 123 417 (or 15.6 per cent) and 140 252 (or 20.5 per cent) particles, respectively, exceeded those limits. Nevertheless, after the $300T_{\rm cr}$ evolution, only 7 (or 0.000 88 per cent) and 112 (or 0.016 per cent) particles from the E2af and E5af models, respectively, were found at a distance from the centre that exceeded that of the initially most distant particle in the corresponding model. Thus, we can conclude that our models are extremely stable over intervals of the order of one Hubble time.

4 FIGURE ROTATION VERSUS MATTER ROTATION

In a non-rotating stellar system, one expects that the outermost particles have approximately zero angular velocity. This is because the external region (halo) of a self-gravitating system in equilibrium, particularly when it is the result of a gravitational collapse, is expected to contain almost all radial or quasi-radial orbits (e.g. Binney & Tremaine 2008, and references therein.). On the other hand, the internal region (core) tends to have particles with a more isotropic distribution of velocities, meaning that there is a wide dispersion of angular velocities in every direction, summing up to zero angular velocity for the system as a whole. Fig. 3 shows that is indeed the

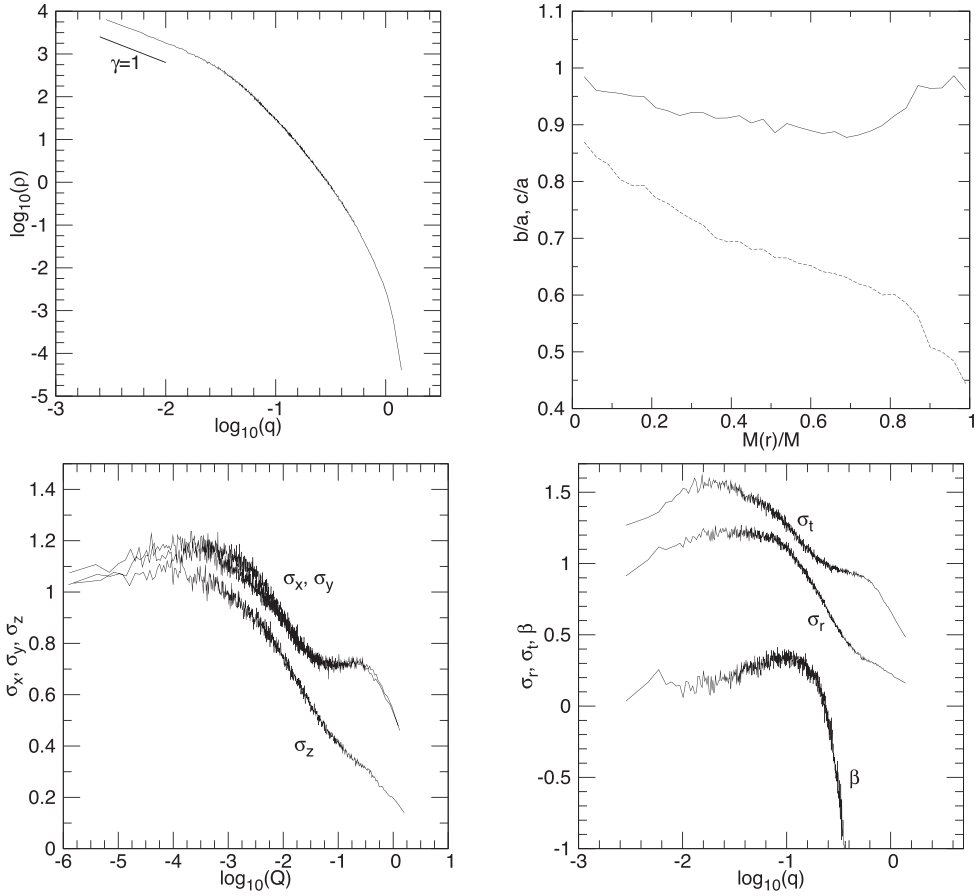

Figure 2. Same as Fig. 1 but for model E5af.

Table 1. Percentage variations over one Hubble time.

Model	ρ_c (per cent)	X (per cent)	Y (per cent)	Z (per cent)	γ (per cent)
E2af	-0.78 ± 0.89	-0.86 ± 0.21	0.91 ± 0.28	0.15 ± 0.29	1.47 ± 1.20
E5af	-0.12 ± 1.04	-1.62 ± 0.18	1.52 ± 0.23	0.54 ± 0.23	-1.60 ± 1.43

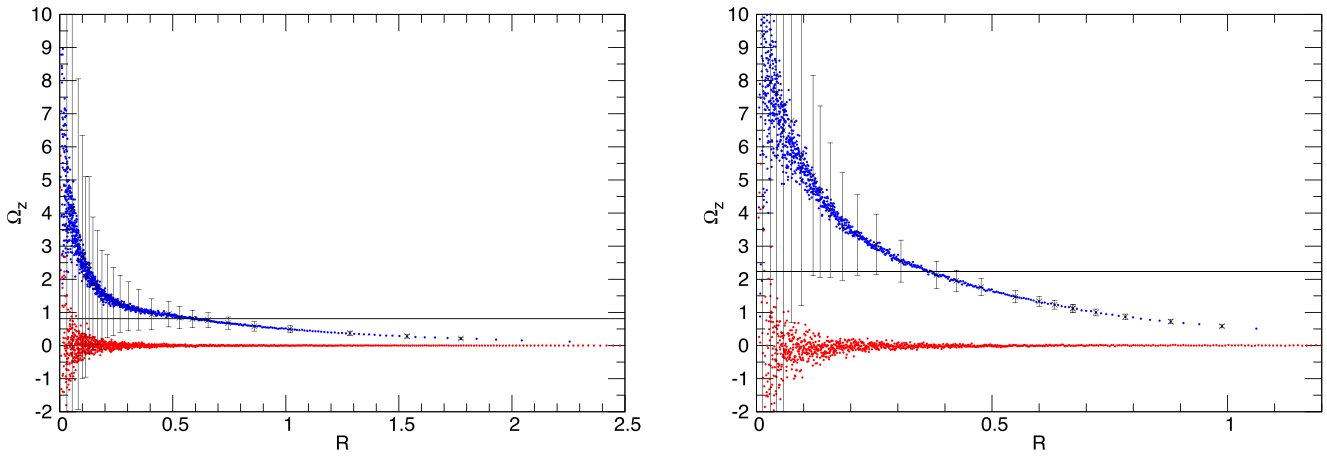

Figure 3. Left: angular velocity Ω_z as function of the cylindrical radius $R = \sqrt{x^2 + y^2}$ for the initial E2a model (lower set of points, red in the electronic version) and for the final E2af model (upper set of points, blue in the electronic version). Each point corresponds to the mean angular velocity of a cylindrical shell containing 1/1000 of the particles. The dispersions within some shells are also shown with bars. A horizontal line at $\Omega = 0.8108$ shows the angular velocity of the figure rotation. Right: the same, but for the E5a and E5af models. The angular velocity of the figure rotation is at 2.2454, marked with an horizontal line. In both cases, the initial models reach $R \simeq 4$.

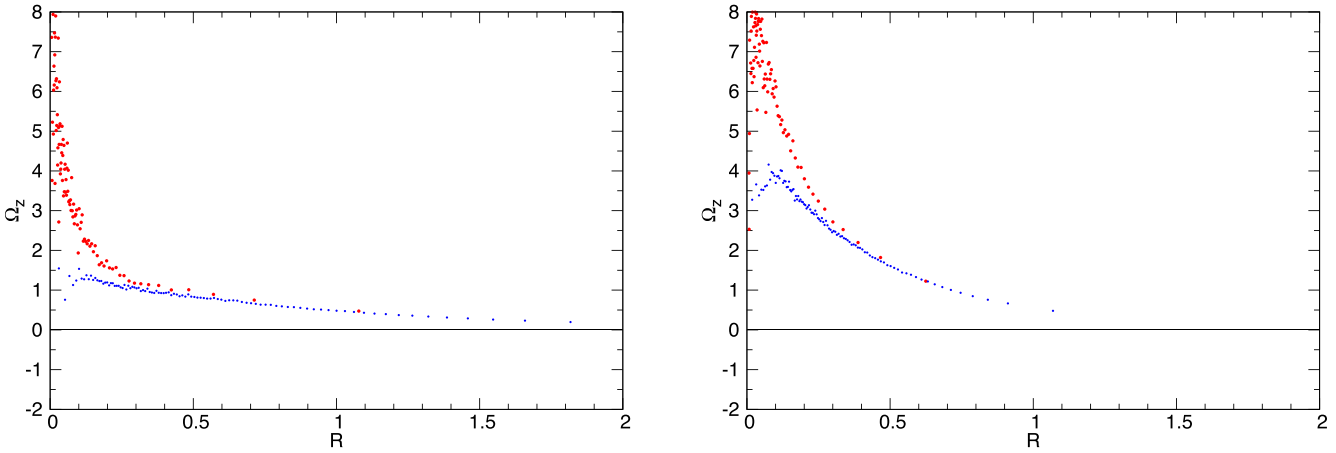

Figure 4. Left: angular velocity Ω_z as function of the cylindrical radius $R = \sqrt{x^2 + y^2}$ for the E2af model, taking only the 20 per cent of particles closest to the equatorial plane (upper set of points, red in the electronic version) and the 20 per cent farthest from that plane (lower set, blue in the electronic version). Each point corresponds to the mean angular velocity of a cylindrical shell containing 1/100 of the corresponding 20 per cent particles. Right: the same, but for the E5af model.

initial state of our E2a and E5a systems (lower sets of points, red in the electronic version).

With the first injection of angular momentum, each particle acquires the same amount of angular velocity, and the resulting profile of $\Omega_z(R)$ (not shown in Fig. 3) is the same as before, but raised by that amount. Therefore, the energy of most of the halo particles exceeds their binding energy and they escape from the system when it is let to evolve. Core particles, on the other hand, tend to remain bound but, as their energy has increased, many will go to populate the halo, thus decreasing their angular velocity due to an approximate conservation of angular momentum. Injection of more angular momentum after this evolution will initially raise again the entire profile without modifying its shape, and the subsequent evolution will yield a new depletion of the halo because of escapes, migration of core particles to the halo, and the lowering of the external profile of $\Omega_z(R)$. The final angular velocity profile of our models, displaying a strong differential rotation, is shown in Fig. 3 (upper sets of points, blue in the electronic version). Moreover, the final rotation also depends on z. Fig. 4 shows the mean angular velocity of cylindrical shells for each final model taking only the 20 per cent of the particles closest to the (x, y) plane (upper sets of points, red in the electronic version) and the 20 per cent farthest from that plane (lower sets, blue in the electronic version). We recall that, in physical units, the unit of abscissae in Figs 3 and 4 corresponds to about 20–40 kpc, for model E2af, and to about 30–70 kpc, for model E5af, and the unit of ordinates to about 4–7 km s^{-1} kpc^{-1}, for model E2a, and to about 2–4 km s^{-1} kpc^{-1}, for model E5af.

These results clearly show that, although the amount of angular velocity imparted to all the particles was the same, the resulting rotation is far from that of a rigid body: the dynamical evolution generates a complex rotation pattern in the models. This turns out to be in sharp contrast with the so-called figure rotation, that is, the rotation of the triaxial shape of the system around its short axis. To measure this rotation, we let our final models evolve for an additional interval of 25 $T_{\rm cr}$, obtaining 10 snapshots, and we analysed each one of these snapshots as follows. First, we sorted all the bound particles according to their energy and distributed them in 20 per cent bins, from the 10 per cent most tightly bound to the 90 per cent most tightly bound, and then we computed for each bin the moments of the inertia tensor and obtained the angle between the semimajor axis of the ellipsoid and the positive x-axis; the 10 per cent less tightly bound and most tightly bound particles were excluded because the corresponding ellipsoids have $b/a \simeq 1.0$ (see Figs 1 and 2, upper right frames) and the angle determination is uncertain. Plots of this angle ϕ versus the elapsed time show the rotation of the ellipsoidal figures, and it was clear that the different energy bins of the figure of each system are rotating with the same angular velocity. We present such plots in Fig. 5, but we only included the innermost and outermost shells for clarity. The angular velocity of this figure rotation, or pattern velocity, was computed using the 80 per cent most tightly bound particles and turned out to be $\Omega_{\rm p} = 0.8108 \pm 0.0054$ and 2.2454 ± 0.0094, respectively, for models E2af and E5af. These values are shown in Fig. 3 with horizontal lines for comparison with the matter rotation and, in physical units, they imply rotation periods between 1.0 and 1.7 Gyr for E2af, and between 0.8 and 1.2 Gyr for E5af.

5 ORBITAL CONTENT OF THE MODELS

We investigated the orbital content of our models with the same methods from the previous papers in this series (Zorzi & Muzzio 2012; Muzzio et al. 2013; Carpintero et al. 2014), that is, Lyapunov exponents to detect chaoticity, and frequency maps to study regular orbits. We used the numerical tools we had developed for those investigations, but we would wish to call the attention of readers new to the field to the software tool SMILE (Vasiliev 2013) that they might find useful.

5.1 Chaoticity

We randomly selected 3961 and 3429 particles, respectively, from models E2af and E5af and we took their positions and velocities as the initial values to obtain the orbits and investigate their chaoticity. The potentials were fixed, keeping constant the coefficients of their expansions, and the integrations were carried out in coordinate systems rotating with the corresponding angular velocities.

Since the potentials were fixed, all our orbits obey the Jacobi integral, and regular orbits have to obey at least two additional isolating integrals, but we can have two kinds of chaotic orbits, partially chaotic orbits that obey only one additional integral, and

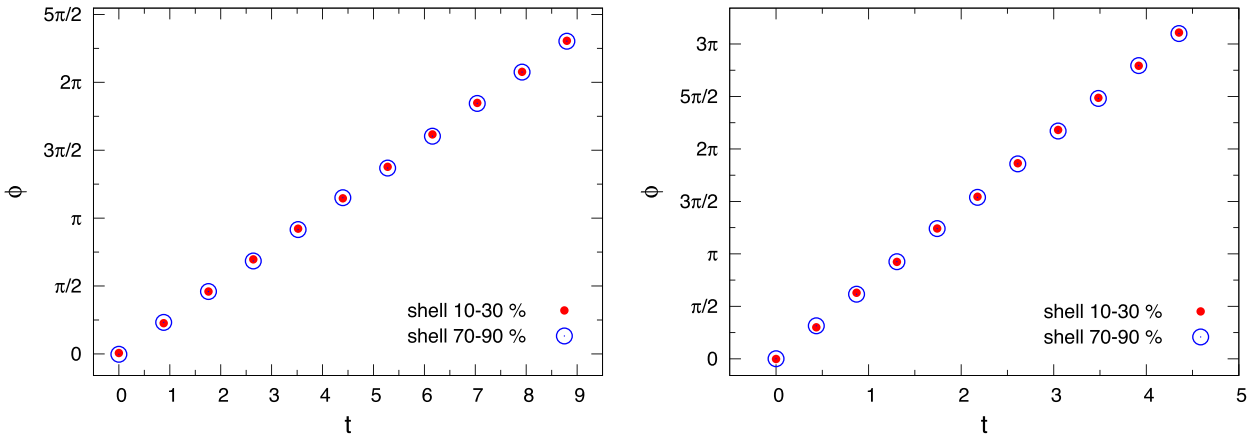

Figure 5. Figure rotation of the E2af (left) and E5af (right) models. Only the results corresponding to two shells containing 20 per cent of the particles are shown for clarity, but the other shells give essentially the same results (see the text). The time spans, expressed in t.u., differ for each model due to the different values of their crossing times, but in both cases they correspond to $25T_{\rm cr}$.

fully chaotic orbits that have no isolating integrals other than the Jacobi integral. Regular, partially and fully chaotic orbits can be classified obtaining the six Lyapunov exponents. Since phase space volume is conserved, the exponents come in three pairs of the same absolute value and opposite sign. The Jacobi integral guarantees that one of those pairs is always zero, and each additional isolating integral makes zero another pair, so that regular orbits have all their Lyapunov exponents equal to zero, partially chaotic orbits have one non-zero pair and fully chaotic orbits have two.

The numerical equivalent of the Lyapunov exponents are the finite time Lyapunov characteristic numbers (hereafter FT-LCNs). As in our previous works, we computed them using the LIAMAG subroutine (Udry & Pfenniger 1988), kindly provided by D. Pfenniger, adopting integration and normalization intervals of 10 000 t.u. and 1 t.u., respectively. We will refer to the largest FT-LCN of a given orbit as $L_{\rm max}$ and to the second largest one as $L_{\rm int}$, hereafter. Since the FT-LCNs are obtained from numerical integrations over a finite time interval, rather than the infinite one required to obtain Lyapunov exponents, they cannot reach zero value, but only a limiting minimum value, $L_{\rm lim}$. As in our previous work, we used plots of the $L_{\rm int}$ versus $L_{\rm max}$ distribution to estimate a value of $L_{\rm lim} = 0.0018\,({\rm t.u.})^{-1}$, the same one obtained by Zorzi & Muzzio (2012). This $L_{\rm lim}$ corresponds to a Lyapunov time of 556 t.u., which is equivalent to about 5 or 6 Hubble times for our models, and one might wonder whether it is reasonable to use such a low $L_{\rm lim}$ to separate regular from chaotic orbits. We have dealt with this matter in our previous work (Aquilano et al. 2007; Muzzio et al. 2009; Zorzi & Muzzio 2012) and we repeat here the same analysis done before, using also a limiting value of $L_{\rm lim} = 0.0100\,({\rm t.u.})^{-1}$ for comparison. First, we separated the orbits of each model into three groups: (a) those with $L_{\rm max} < 0.0018\,({\rm t.u.})^{-1}$, i.e. those that are classified as regular for both choices of $L_{\rm lim}$ (REGREG, hereafter); (b) those with $0.0018\,({\rm t.u.})^{-1} \leq L_{\rm max} < 0.0100\,({\rm t.u.})^{-1}$, i.e. those that are classified as regular for $L_{\rm lim} = 0.0100\,({\rm t.u.})^{-1}$, but as chaotic for $L_{\rm lim} = 0.0018\,({\rm t.u.})^{-1}$ (REGCHAO, hereafter); (c) those with $0.0100\,({\rm t.u.})^{-1} \leq L_{\rm max}$, i.e. those that are classified as chaotic for both elections of $L_{\rm lim}$ (hereafter CHAOCHAO). Then we considered, for each orbit, 11 (x, y, z) orbital positions separated by intervals of 10 t.u., that is, over a total interval of 100 t.u., and, for each model and for each type of orbit, we computed the mean square value of each coordinate. Table 2 gives the square roots of the ratios of the y and z mean square values to the x mean square value.

Table 2. Axial ratios for different $L_{\rm lim}$. Each coordinate x_i stands for $\langle x_i^2 \rangle^{1/2}$.

Model	ratio	REGREG	REGCHAO	CHAOCHAO
E2af	y/x	0.979 ± 0.017	0.987 ± 0.018	0.959 ± 0.020
	z/x	0.543 ± 0.010	0.705 ± 0.013	0.908 ± 0.019
E5af	y/x	1.069 ± 0.024	0.928 ± 0.020	0.957 ± 0.013
	z/x	0.416 ± 0.008	0.499 ± 0.014	0.556 ± 0.007

Table 3. Percentages of chaotic and regular orbits.

Model	Regular	Part. chaotic	Fully chaotic
E2af	25.80 ± 0.70	13.10 ± 0.54	61.10 ± 0.77
E5af	31.93 ± 0.80	10.91 ± 0.53	57.16 ± 0.85

The results in Table 2 show that the y/x ratio of the E5af model and the z/x ratios of both models obtained from the REGCHAO orbits are significantly different, at the 3σ level, from those obtained from the REGREG orbits. We may conclude that orbits with $0.0018\,({\rm t.u.})^{-1} \leq L_{\rm max} < 0.0100\,({\rm t.u.})^{-1}$ have a spatial distribution different from that of regular orbits. Since it is in spatial distribution we are interested here, it is thus reasonable to adopt $L_{\rm lim} = 0.0018\,({\rm t.u.})^{-1}$. Therefore, we classify orbits as regular if $L_{\rm max} < L_{\rm lim}$, as partially chaotic if $L_{\rm int} < L_{\rm lim} \leq L_{\rm max}$ and as fully chaotic if $L_{\rm lim} \leq L_{\rm int}$. The results of the classification are shown in Table 3, where the quoted errors were computed as the dispersions derived from the binomial distribution, i.e. for a percentage p obtained from N data, the dispersion is $\sqrt{p(100-p)/N}$.

As in our previous investigations, chaotic orbits dominate the dynamics of the triaxial models, with less than one-third of the bodies following regular orbits in any of them. A comparison with the results of Zorzi & Muzzio (2012) suggests that chaos might be slightly less important in the present models, but the differences among the structures of those and the present models, from the axial ratios onwards, makes risky any conclusion in this respect. Actually, since rotation implies breaking a symmetry, one might expect to find more chaos in rotating models, as indicated by Muzzio (2006) who, in fact, found slightly more chaos in a very slowly rotating model than in the same model without rotation.

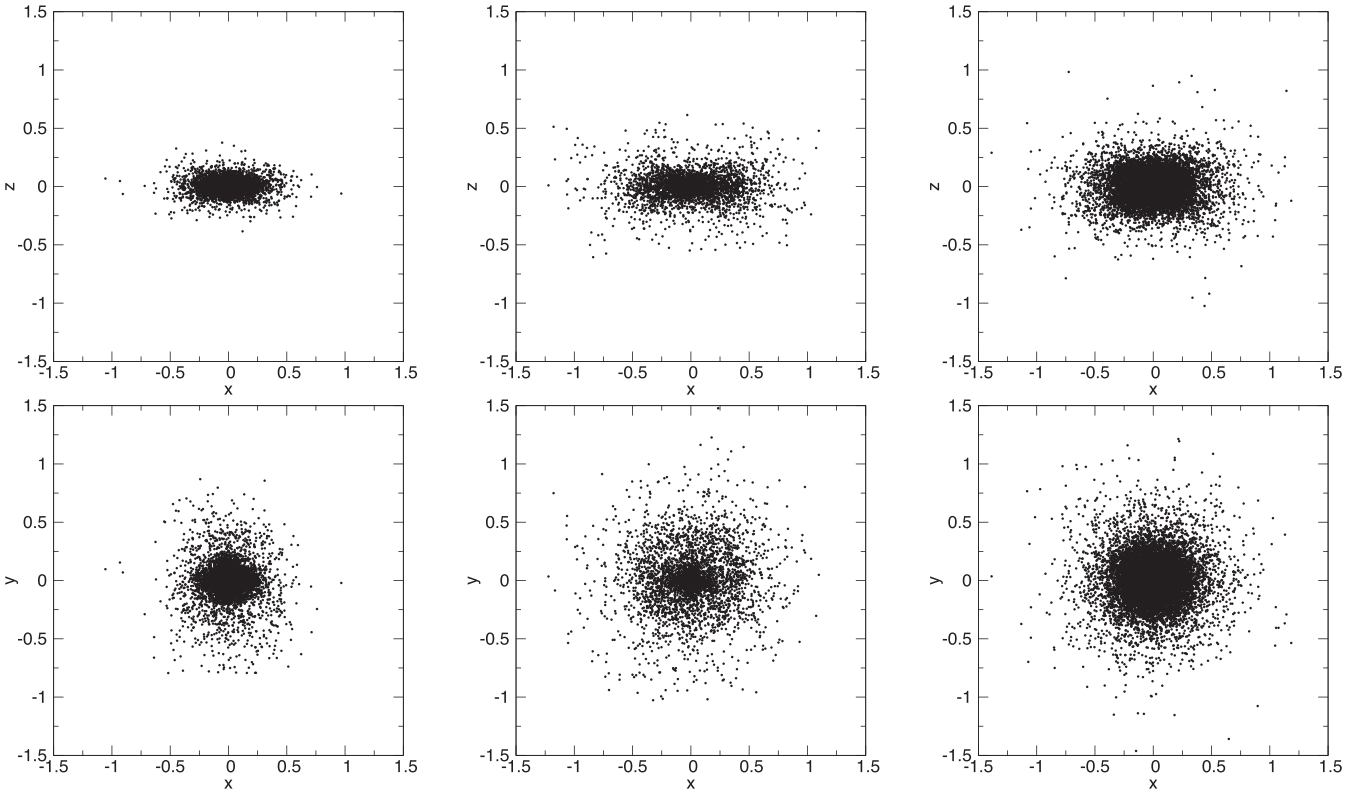

Figure 6. Distribution of the regular (left), partially (centre) and fully chaotic (right) orbits for model E5af.

The long integration interval used to obtain the FT-LCNs allows us to make a further check of the possible escapes searching for those bodies that end up farther from the centre of the system than the farthest body in the original model. We found that, after 10 000 t.u., only 1 body (i.e. 0.03 per cent) on a fully chaotic orbit escapes from the E2af model, while 49 bodies (1.42 per cent) on partially chaotic orbits and 80 bodies (2.33 per cent) on fully chaotic orbits escape from the E5af model, according to this criterium. Two remarks should be made on this respect. First, there is no guarantee that those bodies actually escape because, on the one hand, many of them do not exceed the adopted distance limit by a significant amount and, on the other hand, other bodies alternate shorter and longer distances at intermediate times, i.e. they seem to be on highly elongated rather than on open orbits. Secondly, strictly speaking, a chaotic orbit should have a positive FT-LCN *and* to be bound (e.g. orbits in a repulsive harmonic potential are perfectly regular, in spite of diverging exponentially, but they are unbound), so that the percentages of chaotic orbits of Table 3 might include fractions of unbound orbits that are not chaotic. Nevertheless, those fractions should be exceedingly small in view of our results on the final distances after 10 000 t.u. Moreover, considering that that interval amounts to about 40 Hubble times, we may conclude that escapes are not a serious problem for our models and that they are very stable indeed.

Fig. 6 presents the (x, y) and (x, z) projections of the bodies in the E5af model whose FT-LCN had been computed, separately for those in regular, partially and totally chaotic orbits. To increase the number of points, we have plotted the positions at 10 t.u. intervals over a total integration time of 100 t.u., i.e. 11 points for each orbit. As in our previous investigations on triaxial models, the distribution of the fully chaotic orbits is very different from that of the regular ones, while the partially chaotic orbits adopt a distribution intermediate between the other two. This visual impression is confirmed by the results of Table 4 where we present, for the two models and separately for the regular, partially and fully chaotic orbits, the values of the axial ratios computed from the positions at 10 t.u. intervals from the initial 100 t.u. of the integration interval, i.e. like in Fig. 6. The very different distributions of the regular and fully chaotic orbits is most clearly shown by their different z/x values, although the difference between the corresponding y/x values of the E5af model is also significant at the 3σ level. Partially chaotic orbits have z/x values intermediate between those of the regular and fully chaotic orbits in both models. For the E2af model there are no significant differences, at the 3σ level, among the y/x ratios, but there are very significant ones among the z/x values. At any rate, it is clear that the distributions of the regular, partially and fully chaotic orbits are very different from each other.

Table 4. Axial ratios of regular, partially and fully chaotic orbits. Each coordinate x_i stands for $\langle x_i^2 \rangle^{1/2}$.

Model	Ratio	Regular	Part. chaotic	Fully chaotic
E2af	y/x	0.979 ± 0.017	0.994 ± 0.018	0.942 ± 0.018
	z/x	0.543 ± 0.010	0.679 ± 0.012	0.967 ± 0.019
E5af	y/x	1.069 ± 0.024	0.948 ± 0.021	0.956 ± 0.013
	z/x	0.416 ± 0.008	0.424 ± 0.010	0.602 ± 0.008

5.2 Regular orbits

The frequency analysis was performed, as in our previous papers (Muzzio 2006; Aquilano et al. 2007; Muzzio et al. 2009, 2013; Carpintero et al. 2014), with the modified Fourier transform code of Šidlichovský & Nesvorný (1996, a copy can be obtained at

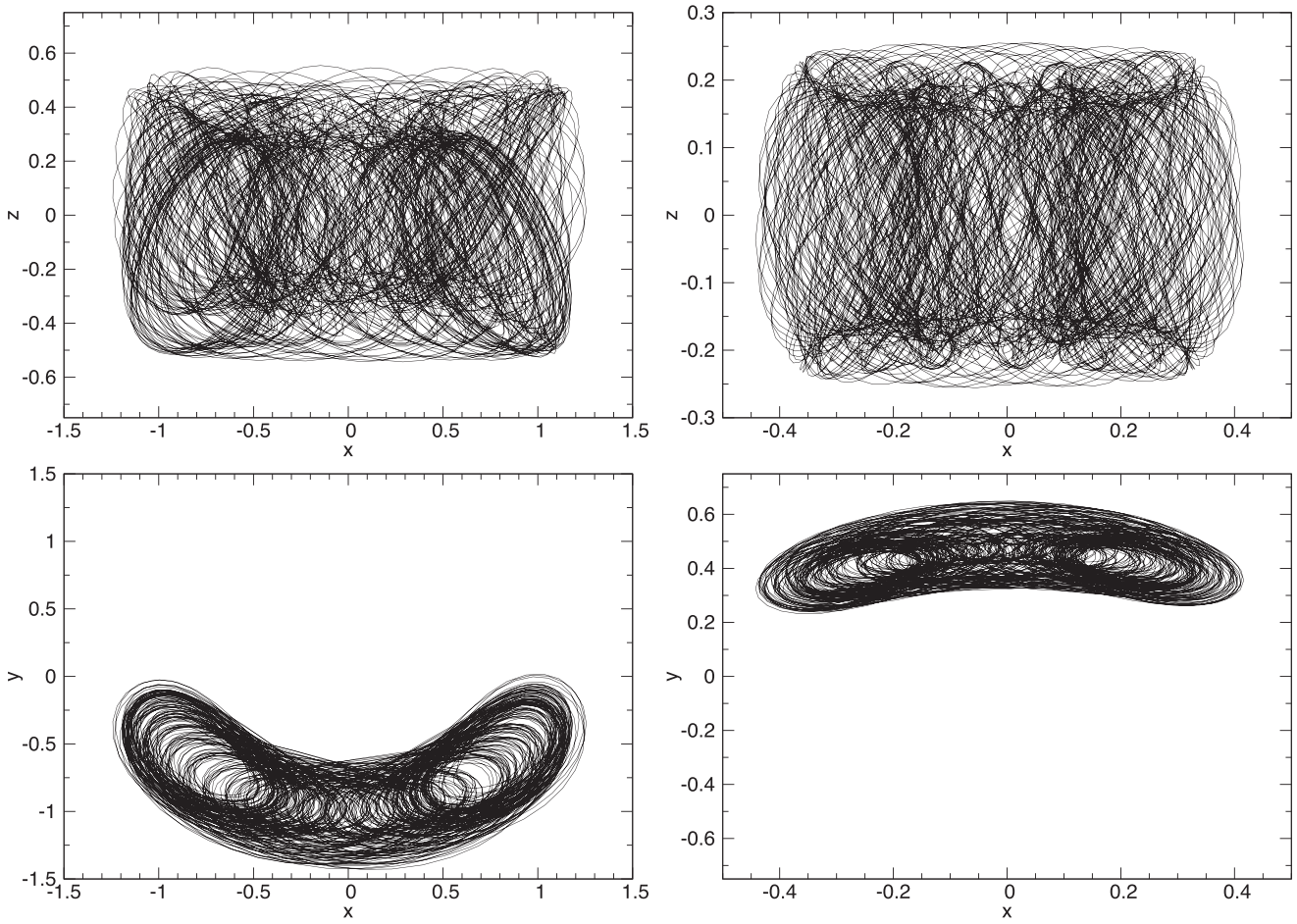

Figure 7. Horseshoe orbits 231 of model E2af (left) and 182 of model E5af (right).

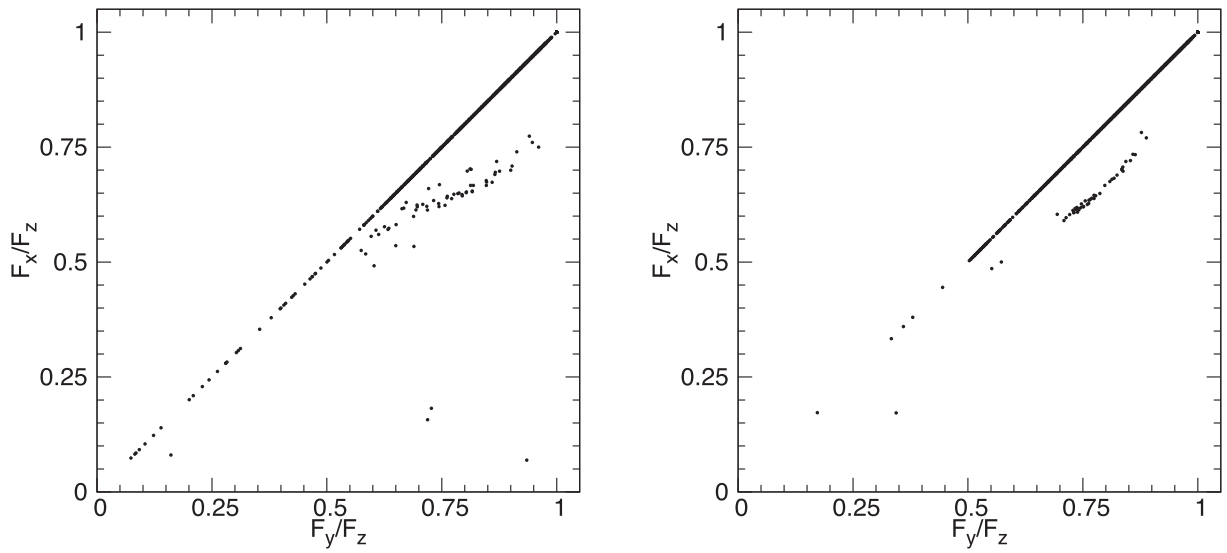

Figure 8. Left: frequency map of the E2af model. Right: frequency map of the E5af model.

www.boulder.swri.edu/~davidn) and adopting as initial conditions the positions and velocities of the same bodies we had selected for the computation of the Lyapunov exponents. For each one of the 2117 regular orbits of the two models, we obtained the fundamental frequencies for each coordinate, F_x, F_y and F_z, through the frequency analysis of the complex variables $x + \mathrm{i}\,\dot{x}$, $y + \mathrm{i}\,\dot{y}$ and $z + \mathrm{i}\,\dot{z}$, respectively; these were derived from 8192 points equally spaced in time obtained integrating the orbits over 300 radial periods. As indicated by Muzzio (2006), the frequencies of isolated lines obtained in this way have errors smaller than 10^{-9}, but the

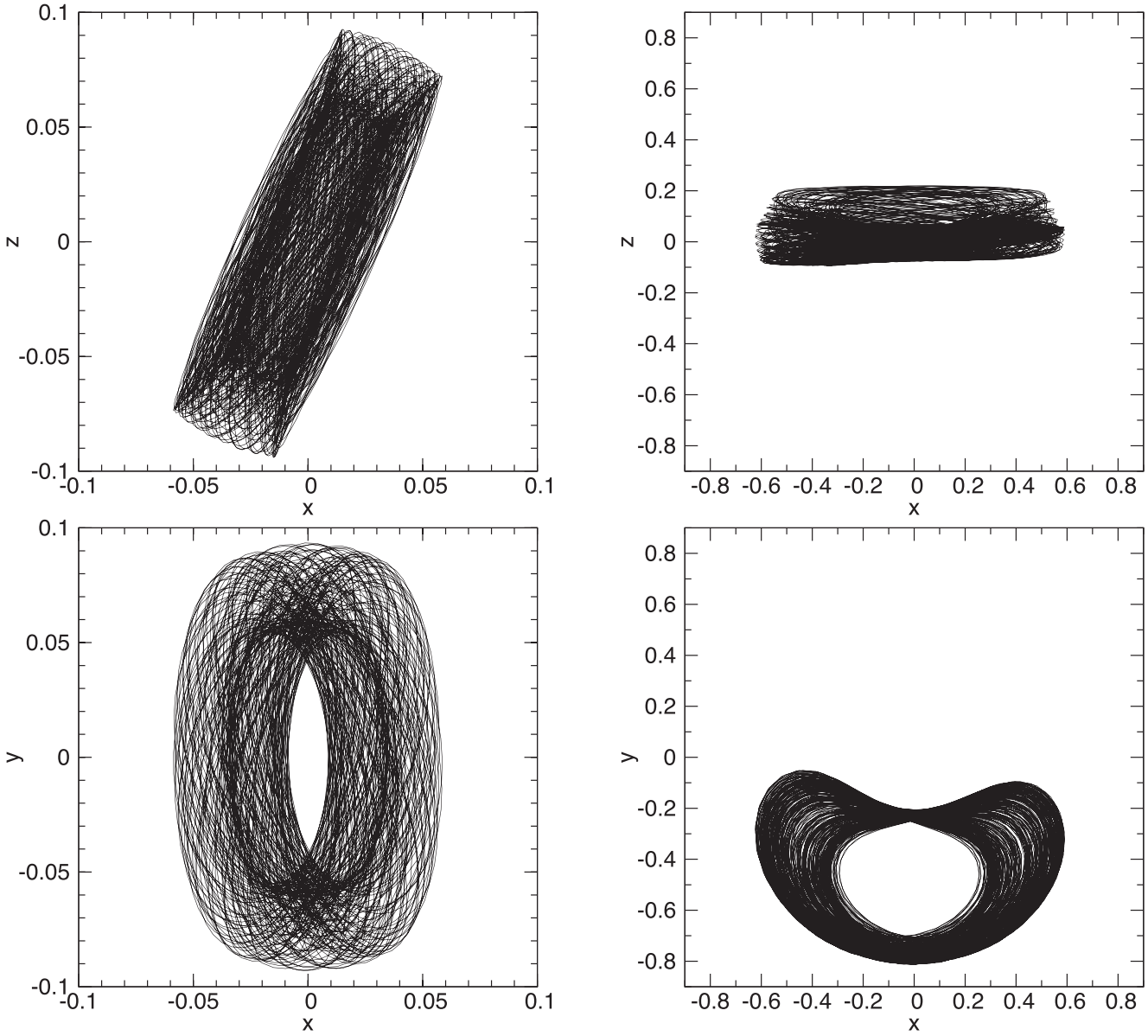

Figure 9. Tilted tube orbit 521 of model E2af (left) and closed horseshoe orbit 177 of model E5af (right).

precision is much lower when there are nearby lines, and here we adopt the practical limit of 2×10^{-4} for the precision, as in our previous works.

We obtained the fundamental frequencies using the method of Kalapotharakos & Voglis (2005) with the improvements introduced by Muzzio (2006), Aquilano et al. (2007) and Muzzio et al. (2009). The original method took the frequency of the largest amplitude in each coordinate as the fundamental frequency for that coordinate but, as shown by Binney & Spergel (1982) and Muzzio (2006), respectively, the libration of some orbits and the extreme elongation of others makes necessary to adopt, for these cases, other frequencies as the fundamental ones, and the improvements deal with those cases.

In our previous work on non-, or very slowly, rotating systems, the fundamental frequencies were used to classify the regular orbits as LATs and SATs, respectively and boxes and boxlets (BBLs), but the orbital composition of rotating systems is much more varied and complex (see e.g. Binney & Tremaine 2008) and that classification is not enough. Besides, although it is not unfrequent to find those same names used for orbits in rotating systems, it should be recalled that things are quite different in fixed and rotating systems of reference (e.g. a BBL in one system may be a SAT in another one). As we will see below, most of the regular orbits in our models are resonant, i.e. their fundamental frequencies obey one or two equations of the form:

$$l F_x + m F_y + n F_z = 0, \tag{7}$$

with l, m and n integers not all equal to zero. Therefore, in what follows we will refer to the different orbits mainly by their resonances, i.e. (l, m, n) in the equation above. Besides, we will not restrict ourselves to frequency analysis and we will add other criteria (like the conservation of the signs of the components of the angular momentum and plots of the orbits) to aid the orbital classification.

Of the 2117 orbits regarded as regular, 122 yielded values of their fundamental frequencies that did not obey that $F_x \leq F_y \leq F_z$. As in our previous works, visual inspection of their spectra

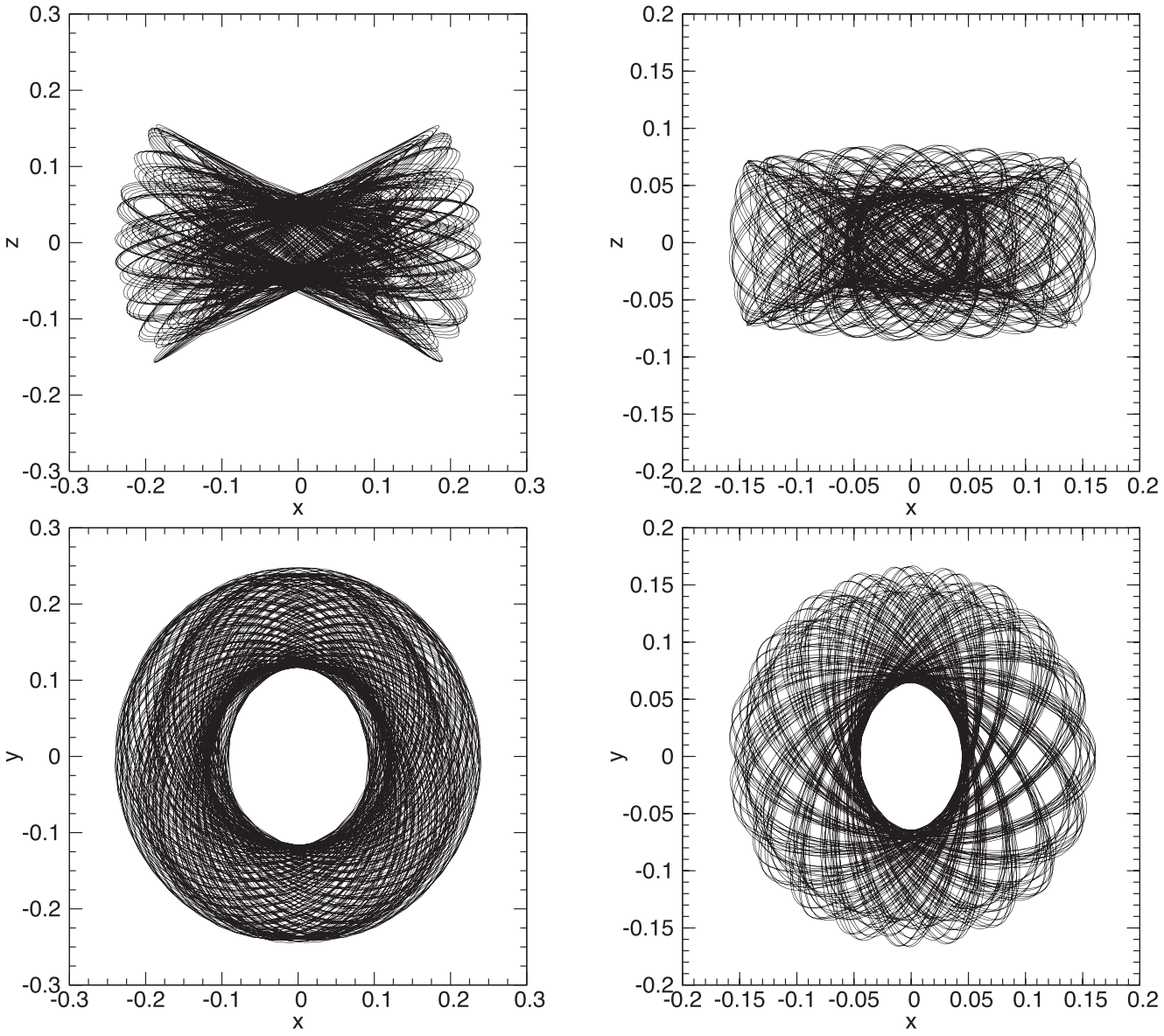

Figure 10. Two SATs: orbits 76 of model E2af (left) and 20 of model E5af (right).

showed that many of them were typical of chaotic orbits, with lines of similar frequencies and amplitudes. We checked that possibility obtaining the FT-LCNs of those orbits using an integration time of 100 000 t.u., i.e. 10 times longer than the one of Subsection 5.1, and 44 of the 122 suspicious orbits turned out to be actually chaotic. Besides, it should be recalled that in rotating systems there are orbits whose fundamental frequencies might not be obtained with the same criteria used for non-rotating ones. For example, another 11 of those 78 orbits had a frequency line with F_y close to zero, i.e. they were horseshoe orbits (two examples are shown in Fig. 7).

Fig. 8 presents the frequency maps for both models. Orbits that do not obey $F_x \leq F_y \leq F_z$, mentioned above, are not included, but we notice four cases of model E2af and one of model E5af in odd positions of the diagrams. Orbit 2166 of model E2af, at $(F_y/F_z, F_x/F_z) = (0.161, 0.080)$, and orbit 773 of model E5af, at (0.344, 0.172), are just horseshoes. Visual inspection of the frequency spectra of orbits 1706, at (0.727, 0.182), and 1870, at (0.719, 0.157), of model E2af showed that they are very complex, making very difficult to select the fundamental frequencies. Plots of those orbits suggest that they are boxlets that avoid the centre of the system; besides, they do not conserve the sign of the components of the angular momentum and both obey the (1, −3, 2) resonance. The frequency spectrum of orbit 3390 of model E2af, at (0.935, 0.069), was clearly chaotic and the chaoticity of that orbit was confirmed recomputing its FT-LCNs with a 100 000 u.t. interval.

The most striking feature of Fig. 8 is the complete lack of representative points at $F_y/F_z \simeq 1.0$ for $F_x/F_z < 1.0$, i.e. the (0, 1, −1) resonant orbits, or the LATs of non-rotating systems. Nevertheless, the points at $F_y/F_z \simeq 1.0$ and $F_x/F_z \simeq 1.0$ are not single points but each one includes many orbits (35 for model E2af and 61 for model E5af) that obey both the (1, −1, 0) and (0, 1, −1) resonances. All those from the E2af model conserve the sign of the x component of the angular momentum, but only 13 of them conserve the sign of the z component as well: they are tubes with their axes in the (x, z) plane, but not in the (x, y) plane, i.e. they are inclined with respect to the latter plane, and the conservation of the sign of the z

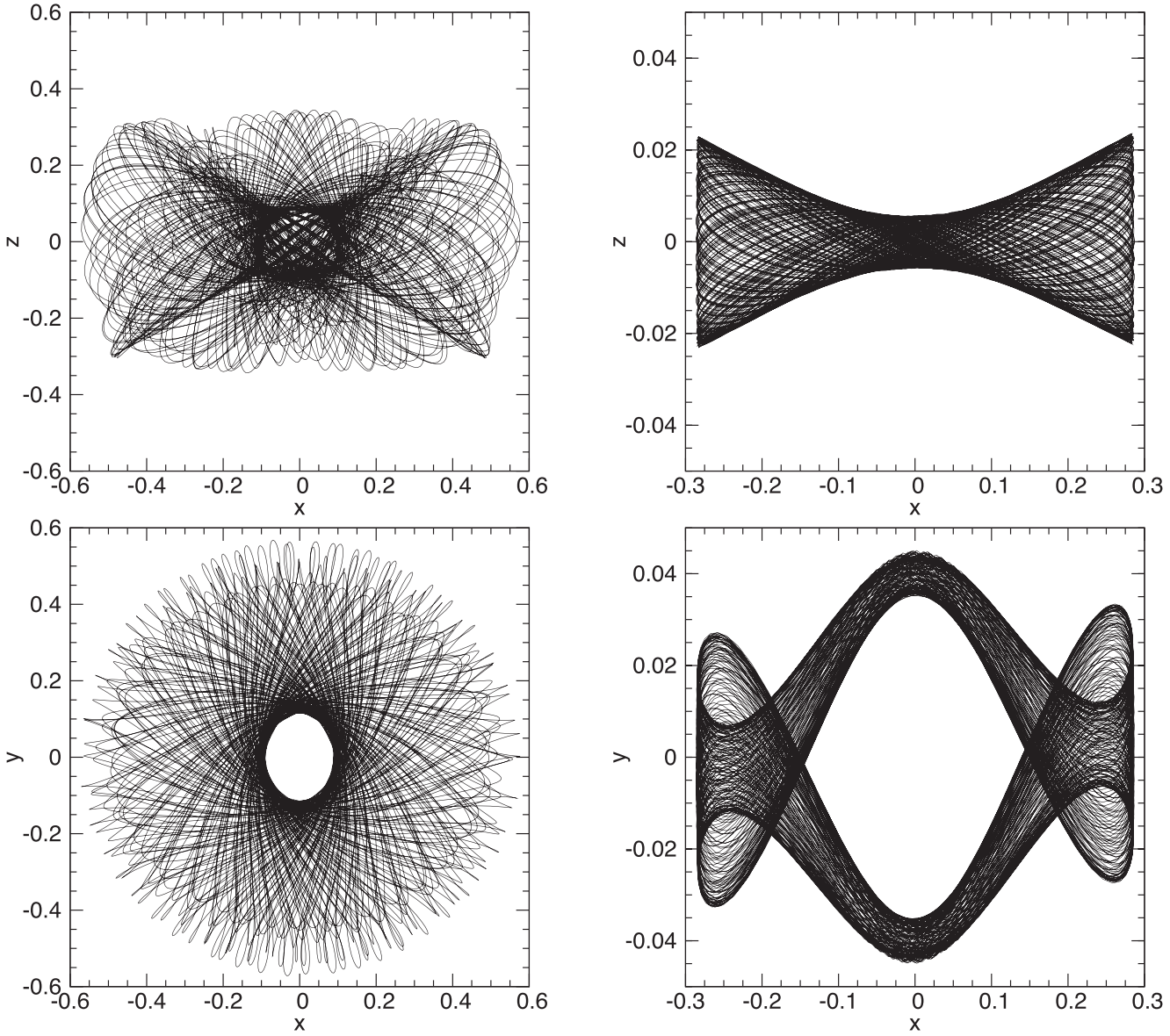

Figure 11. Two orbits that cross themselves: orbits 1855 of model E2af (left) and 142 of model E5af (right); notice that, for the latter, the scales of the y- and z-axes are very different than that of the x-axis, because the orbit is strongly elongated.

component depends on the tilt and the width of the tube. An example is shown on the left-hand side of Fig. 9. 59 of the 61 cases of the E5af model are also tilted tubes like those of model E2af, but their tilts and widths are such that all conserve the signs of both the x and z components of the angular momentum. The remaining two cases do not conserve the sign of the x component of the angular momentum and plots of those orbits showed that they are tubes around the Lagrangian point L5, or like horseshoes long enough to close on to themselves. In fact, when the angular momentum is computed with respect to L5, the sign of its z component is conserved for those orbits. One of them is shown on the right-hand side of Fig. 9.

Another interesting feature of our frequency maps is that they are dominated by the diagonal $F_x/F_z \simeq F_y/F_z$, i.e. the (1, −1, 0) resonance, that in non-rotating systems corresponds to the SATs. In fact, most of the orbits in those diagonals in Fig. 8 are also SATs: after excluding those with $F_y/F_z \simeq 1.0$ and the horseshoes mentioned above, there remain 857 in model E2af and 916 in model E5af, with 591 of the former and 802 of the latter conserving the sign of the z component of the angular momentum, i.e. they are SATs as shown in the two examples of Fig. 10. Most of the rest, i.e. the orbits that do not conserve the sign of the z component of the angular momentum, are also SATs that cross themselves simply because they are in a rotating system, as shown on the left-hand side of Fig. 11, but there are also some of the type shown, e.g. in fig. 3.19 of Binney & Tremaine (2008), as shown on the right-hand side of our figure. A search for additional resonances, with $|l|$, $|m|$ and $|n|$ not larger than 10, among the orbits on the $F_x/F_z \simeq F_y/F_z$ line yielded only 22 in model E2af and 25 in model E5af, most of them of high order.

Except for the few cases with low F_x/F_z values mentioned above, the points falling outside the $F_x/F_z \simeq F_y/F_z$ lie in the region occupied by the BBLs of non-rotating models (see e.g. fig. 1 of Muzzio et al. 2013), but most of them are more similar to orbits like that shown on the right-hand side of Fig. 11 than to boxes; two

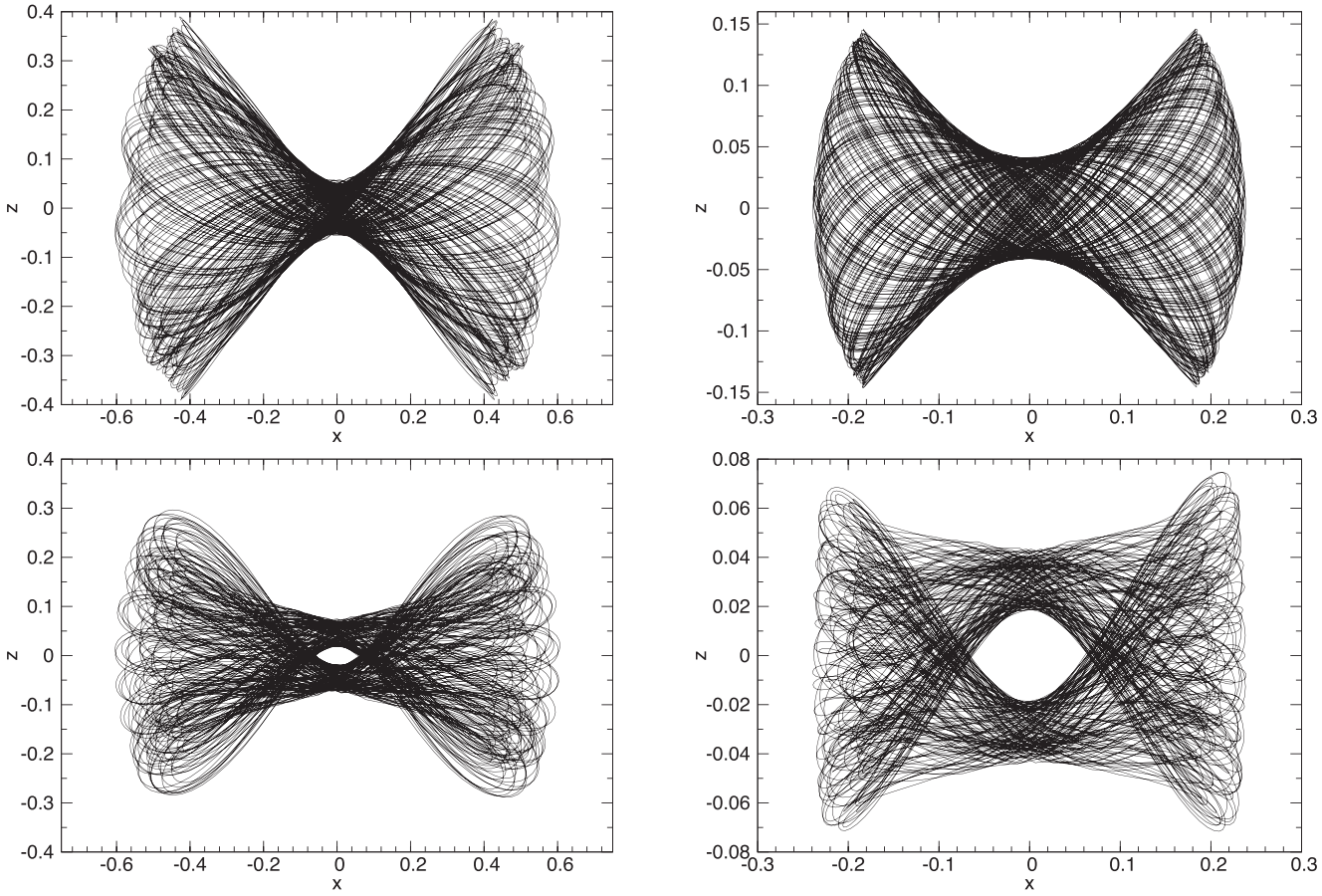

Figure 12. Two orbits lying outside the (1, −1, 0) resonance: orbits 304 of model E2af (left) and 468 of model E5af (right).

examples are shown in Fig. 12. A search for resonances, with $|l|$, $|m|$ and $|n|$ not larger than 10, among these orbits found that 34 out of 63 of model E2f, and 26 out of 47 of model E5af obeyed at least one, but there does not seem to be any one particularly frequent or relevant; two examples of these resonant orbits are shown in Fig. 13.

6 CONCLUSIONS

We have shown here that it is possible, starting from a non-rotating self-consistent *N*-body model of a triaxial and cuspy stellar system, to create a similar rotating one by adding rotation to its particles and letting it to relax towards a new equilibrium. The outcome is a system with differential rotation, with the angular velocity depending both on the distance to the centre and on the height above the equatorial plane, but with a very uniform figure rotation. Besides, these models are highly stable over intervals of the order of a Hubble time.

Zorzi & Muzzio (2012) had shown that the density distribution of their models mimics that of elliptical galaxies and our Figs 1 and 2 (upper left) show the same for the present models. The rotation of our models can be compared with the results of Emsellem et al. (2007) who define a global rotation parameter λ_R that, in their Appendix A, they related to our λ by

$$\lambda \simeq \frac{\sqrt{2}}{3}\lambda_R. \qquad (8)$$

The corresponding values for our models E2af and E5af are, thus, $\lambda_R = 0.263$ and $\lambda_R = 0.378$, respectively, and one can find several examples of real galaxies with similar values in the table 1 of Emsellem et al. (2007). Besides, Copin, Cretton & Emsellem (2004) adjusted an axisymmetric model to SAURON (Bacon et al. 2001) data on NGC 3377 and they computed the velocity dispersions of their model at different points on the meridian plane. Using their reported distance to NGC 3377 (9.9 Mpc) to transform their angular distances into linear ones, and computing the anisotropy from the curves of their fig. 13, it turns out to be of the same order of magnitude than our own values.

To investigate figure rotation observations alone are not enough and models have to be fitted to them. Statler et al. (2004) did this for the old elliptical NGC 4365 and they found hints of figure rotation, roughly estimating a period of about 5 Gyr, somewhat longer than for our models. It should be noted, however, that their model rotates about the semimajor axis, rather than the small axis as our models do. Interestingly, they found that NGC 4365 is triaxial, with $T \simeq 0.45$, i.e. very similar to the triaxiality of our model E2af ($T = 0.447$).

About two-thirds of the orbits in our models are chaotic and bodies on regular, partially and fully chaotic orbits have different spatial distributions. The elliptical galaxies that our chaotic models represent would have rotation periods within 10^8–10^9 yr range, thus confirming the suggestion of Deibel et al. (2011) that unstable orbits appear within that range. Nevertheless, we cannot agree with their statement that stable systems are unlikely to have rotation speeds that produce a high level of stochasticity, as our own models prove

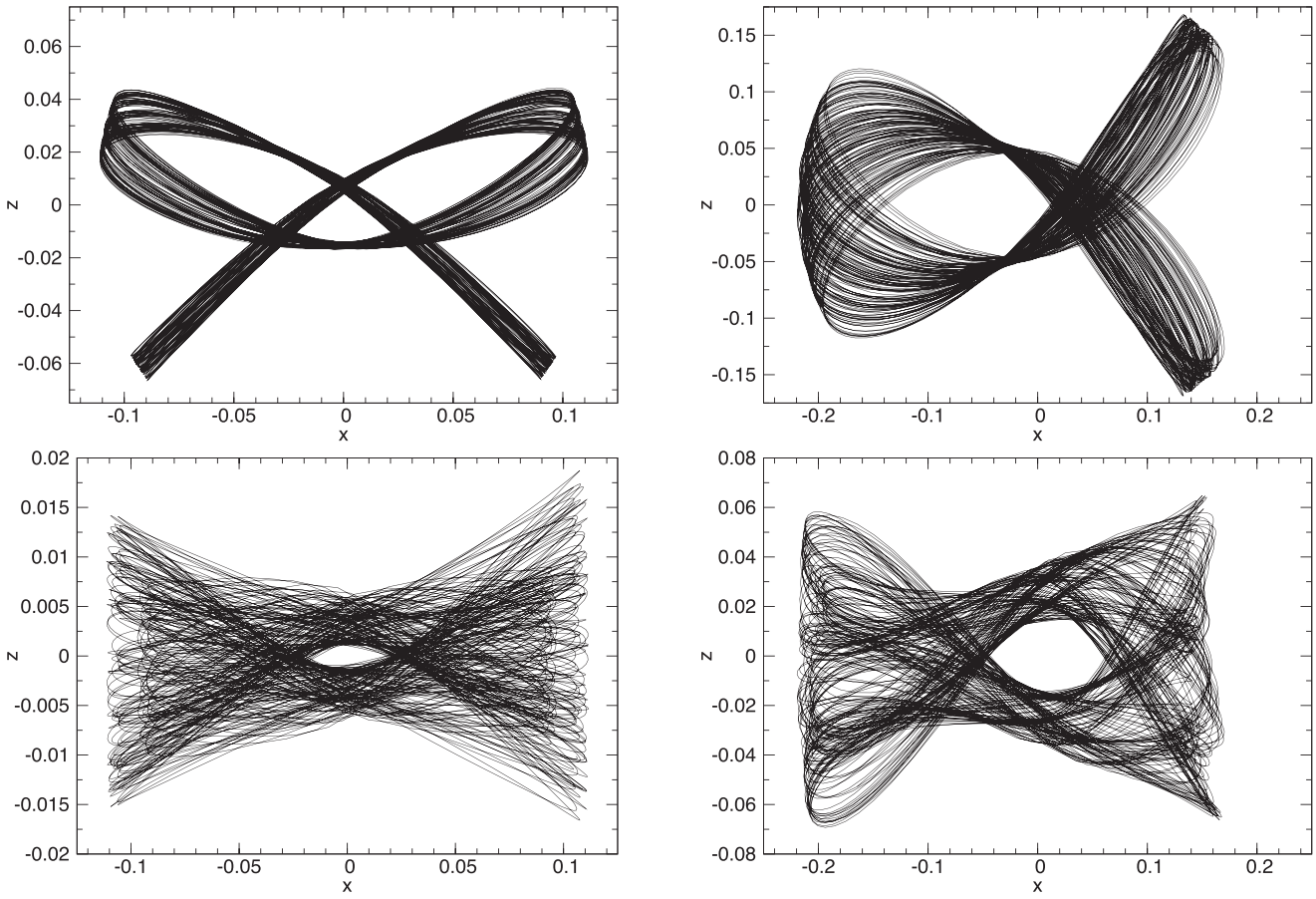

Figure 13. Two resonant orbits lying outside the (1, −1, 0) resonance: orbits 2692 of model E2af (left) and 2164 of model E5af (right); the former is a pretzel that obeys the resonance (4, 0, −3), and the latter a fish that obeys the resonance (3, 0, −2).

otherwise. We had shown in our previous investigations that non-, or very slowly, rotating triaxial stellar models with very high fractions of chaotic orbits can be perfectly stable; now this work extends that conclusion to rotating models as well.

Regular families are dominated by far by the SATs. The fractions of BBLs are low as are those of horseshoes and orbits that cross themselves, typical of rotating systems. The LATs are replaced by tubes whose axes lie on the short-long axes plane, but do not coincide with the major axis.

Finally, it is interesting to compare our frequency maps with those of Deibel et al. (2011), who investigated sample orbits in a rotating triaxial Dehnen (1993) potential, i.e. without considering self-consistency. Thus, it is not surprising that our Fig. 8 shows significant empty spaces in regions where their figs 2, 3, 7, and 10 are well populated. It is simply the result that not all *possible* orbits will be *actually* present in a self-consistent model, because self-consistency imposes a strong selection effect, a fact beautifully proved by Kalapotharakos & Voglis (2005).

ACKNOWLEDGEMENTS

We are very grateful to L. Hernquist, D. Nesvorný and D. Pfenniger for allowing us to use their codes, and to R.E. Martínez and to H.R Viturro for their technical assistance. The comments of an anonymous referee were very useful to improve the original version of this paper, and the assistance of M. Muzzio to improve the English of that version is gratefully acknowledged. This work was supported with grants from the Consejo Nacional de Investigaciones Científicas y Técnicas de la República Argentina, the Agencia Nacional de Promoción Científica y Tecnológica and the Universidad Nacional de La Plata.

REFERENCES

Aquilano R. O., Muzzio J. C., Navone H. D., Zorzi A. F., 2007, Celest. Mech. Dyn. Astron., 99, 307
Bacon R. et al., 2001, MNRAS, 326, 23
Bertola F., Capaccioli M., 1975, ApJ, 200, 439
Binney J., Spergel D., 1982, ApJ, 252, 308
Binney J., Tremaine S., 2008, Galactic Dynamics, 2nd edn. Cambridge Univ. Press, Cambridge
Carpintero D. D., Muzzio J. C., Navone H. D., 2014, MNRAS, 438, 2871
Copin Y., Cretton N., Emsellem E., 2004, A&A, 415, 889
Crane P. et al., 1993, ApJ, 106, 1371
Dehnen W., 1993, MNRAS, 265, 250
Deibel A. T., Valluri M., Merritt D., 2011, ApJ, 728, 128
Dubinski J., Carlberg R., 1991, ApJ, 378, 496
Emsellem E. et al., 2007, MNRAS, 379, 401
Forbes D. A., Ponman T. J., 1999, MNRAS, 309, 623
Hernquist L., 1990, ApJ, 356, 359
Hernquist L., Barnes J., 1990, ApJ, 349, 562
Hernquist L., Ostriker J. P., 1992, ApJ, 386, 375
Holley-Bockelmann K., Mihos J. C., Sigurdsson S., Hernquist L., 2001, ApJ, 549, 862
Illingworth G., 1977, ApJ, 218, L43
Kalapotharakos C., Voglis N., 2005, Celest. Mech. Dyn. Astron., 92, 157

Kandrup H. E., Siopis C., 2003, MNRAS, 345, 727
Merritt D., Fridman T., 1996, ApJ, 460, 136
Moller P., Stiavelli M., Zeilinger W. W., 1995, MNRAS, 276, 979
Muzzio J. C., 2006, Celest. Mech. Dyn. Astron., 96, 85
Muzzio J. C., Carpintero D. D., Wachlin F. C., 2005, Celest. Mech. Dyn. Astron., 91, 173
Muzzio J. C., Navone H. D., Zorzi A. F., 2009, Celest. Mech. Dyn. Astron., 105, 379
Muzzio J. C., Navone H. D., Zorzi A. F., 2013, MNRAS, 428, 2995
Napolitano N. R. et al., 2005, MNRAS, 357, 691
Peebles P. J. E., 1971, A&A, 11, 377
Ryden B. S., 1996, ApJ, 461, 146
Schwarzschild M., 1979, ApJ, 232, 236
Schwarzschild M., 1982, ApJ, 263, 599
Schwarzschild M., 1993, ApJ, 409, 563
Šidlichovský M., Nesvorný D., 1996, Celest. Mech. Dyn. Astron., 65, 137
Siopis C., Kandrup H. E., 2000, MNRAS, 319, 43
Sparke L. S., Sellwood J. A., 1987, MNRAS, 225, 653
Statler T. S., Emsellem E., Peletier R. F., Bacon R., 2004, MNRAS, 353, 1
Udry S., Pfenniger D., 1988, A&A, 198, 135
Vasiliev E., 2013, MNRAS, 434, 3174
Vasiliev E., Athanassoula E., 2012, MNRAS, 419, 3268
Vasiliev E., Athanassoula E., 2015, MNRAS, 450, 2842
Voglis N., Kalapotharakos C., Stavropoulos I., 2002, MNRAS, 337, 619
Zorzi A. F., Muzzio J. C., 2012, MNRAS, 423, 1955

This paper has been typeset from a TEX/LATEX file prepared by the author.